Supporting Information for

Magnetic Coupling between Fe(NO) Spin Probe Ligands Through Diamagnetic Ni^{II}, Pd^{II} and Pt^{II} Tetrathiolate Bridges

Manuel Quiroz,[a] Molly M. Lockart,[b] Shan Xue,[c] Dakota Jones,[a] Yisong Guo,[c] Brad S. Pierce,[d] Kim R. Dunbar,[a*] Michael B. Hall,[a*] and Marcetta Y. Darensbourg [a*]

[a]Department of Chemistry, Texas A & M University, College Station, Texas 77843, United States

[b]Department of Chemistry & Biochemistry, Samford University, Birmingham, Alabama 35229, United States

[c]Department of Chemistry, Carnegie Mellon University, Pittsburgh, Pennsylvania 15213, United States

[d]Department of Chemistry & Biochemistry, University of Alabama, Tuscaloosa, Alabama 35487, United States

Table of Contents

Materials and Methods……**S2-7**

Infrared and UV-Vis spectroscopy……**S8**

Positive-ion ESI-MS data with isotopic bundles……**S9**

Zero field ^{57}Fe Mössbauer spectroscopy with simulation parameters……**S10**

Electrochemical data from cyclic voltammograms over multiple scan rates……**S11-12**

SQUID magnetometry data with fits (χ_M vs. T and $1/\chi_M$ vs. T plots)……**S12**

Crystallographic refinement details……**S13**

X-ray crystal structures and packing diagrams……**S14-16**

Selected bond length and angles from x-ray crystal structures……**S17-20**

Frontier orbital energy diagrams……**S21**

Frontier orbital contour plots……**S22**

Spin Density plots……**S23**

Comparison of the transoid and cisoid optimized structures……**S24**

Computational Coordinates (optimized BS singlet)……**S25-27**

References ……**S28**

Materials and Methods

General Considerations. All reactions were performed in a N_2 atmosphere glovebox or by using standard Schlenk line technique. All solvents were purified with an MBraun Manual Solvent Purification System with AcloaF200 activated alumina dessicant. All reagents were purchased from Sigma Aldrich, TCI, and BTC, and used as received. The starting material N,N-bis(2-mercaptoethyl)-1,4-diazacycloheptane (bme-dach), (NO)Fe(bme-dach), was synthesized according to published procedures.[1] The $[Pt(CH_3CN)_4][BF_4]$ precursor was prepared from a modified procedure which involves the protonation of $Pt(acac)_2$ with excess $HBF_4{\bullet}Et_2O$ (20 equivalents) in CH_3CN. The $[n\text{-}Bu_4N][PF_6]$ and $AgNO_3$ salts were reagent grade and used as purchased from Sigma Aldrich.

A Bruker Tensor Fourier Transform IR (FTIR) spectrometer was used to acquire infrared spectra with a CaF_2 cell. Electronic absorption spectra were obtained using a Shimadzu UV-1601PC spectrophotometer. The Laboratory for Biological Mass Spectrometry at Texas A&M Univeristy was used to collect mass spectrometry (ESI-MS) data. Elemental analyses were performed at Atlantic Microlab Inc. in Norcross, Ga. Zero-field ^{57}Fe Mössbauer spectra were collected on a SEE Co. Mössbauer spectrometer (MS4) with a $^{57}Co/Rh$ radiation source and the spectra were fitted with the WMOSS software (both from SEE co.).

Synthesis of $[(NO)Fe(bme\text{-}dach)\text{-}Pd^{II}\text{-}(bme\text{-}dach)Fe(NO)][BF_4]_2$, $[FePdFe][BF_4]_2$. In a small vial, 36 mg (0.082 mmol) of $[Pd(CH_3CN)_4][BF_4]_2$ was dissolved in approximately 5 mL of CH_3CN. In a large vial, 50 mg (0.164 mmol) of (NO)Fe(bme-dach) was dissolved in approximately 10 mL of CH_3CN and the solution of $[Pd(CH_3CN)_4][BF_4]_2$ was added dropwise and stirred for 45 mins. The color of the solution gradually changed from dark green to yellow-green as the reaction approached completion. The solution was concentrated and excess Et_2O was added to precipitate the product. The solid product was redissolved in CH_3CN and filtered through Celite. Dark green

crystals of the product were grown using vapor diffusion of Et_2O into a solution of CH_3CN at room temperature to yield 65 mg of product (~ 90 % yield). FTIR (CaF2 windows, CH_3CN, 23 °C): ν(NO) = 1734 cm^{-1} (s). UV-vis absorption spectrum [CH_3CN, λ_{max}, nm (ε_M, M^{-1} cm^{-1})]: 387 (9070), 413 (9440), 600 (600). Cyclic voltammetry in CH_3CN: **[FePdFe]$^{2+}$** + e^- → **[FePdFe]$^+$** (-0.76 V), **[FePdFe]$^+$** + e^- → **[FePdFe]^0** (-1.01 V). ESI-MS positive mode: $[M]^{2+}$ = 356.97 m/z. Anal. Calcd for $H_{42}C_{22}O_2N_8S_4Fe_2B_2F_8Pd$: H, 4.36 C, 27.22; N, 11.55; S, 13.21. Found: H, 4.44; C, 26.62; N, 10.68; S, 13.55.

Synthesis of [(NO)Fe(bme-dach)-Ni^{II}-(bme-dach)Fe(NO)][BF$_4$]$_2$, [FeNiFe][BF$_4$]$_2$. This nickel analogue was prepared in a similar manner as described above for **[FePdFe][BF$_4$]$_2$** except $[Ni(CH_3CN)_4][BF_4]_2$ was generated *in situ* by dissolving 28 mg (0.082 mmol) of $Ni(BF_4)$•$6H_2O$ in CH_3CN and stirring for 30 mins before addition to (NO)Fe(bme-dach) (50 mg, 0.164 mmol). Dark yellow crystals of the product were grown using vapor diffusion of Et_2O into a solution of CH_3CN at room temperature to yield 60 mg of product (~ 88 % yield). FTIR (CaF2 windows, CH_3CN, 23 °C): ν(NO) = 1734 cm^{-1} (s). UV-vis absorption spectrum [CH_3CN, λ_{max}, nm (ε_M, M^{-1} cm^{-1})]: 415 (8420), 625 (595). Cyclic voltammetry ($E_{1/2}$): **[FeNiFe]$^{2+}$** + e^- → **[FeNiFe]$^+$** (-0.85 V), **[FeNiFe]$^+$** + e^- → **[FeNiFe]^0** (-1.06 V). ESI-MS positive mode: $[M]^{2+}$ = 332.99 m/z. Anal. Calcd for $H_{42}C_{22}O_2N_8S_4Fe_2B_2F_8Ni$: H, 4.59; C, 28.63; N, 12.14; S, 13.90. Found: H, 4.62; C, 28.46; N, 11.26; S, 13.95.

Synthesis of [(NO)Fe(bme-dach)-Pt^{II}-(bme-dach)Fe(NO)][BF$_4$]$_2$, [FePtFe][BF$_4$]$_2$. This platinum analogue was prepared in a similar manner as described above for **[FePdFe][BF$_4$]$_2$** using 28 mg (0.056 mmol) of freshly prepared $[Pt(CH_3CN)_4][BF_4]_2$ and 34 mg (0.114 mmol) of (NO)Fe(bme-dach). Brown crystals of the product were grown using vapor diffusion of Et_2O into a solution of CH_3CN at room temperature to yield 33 mg of product (~ 60 % yield). FTIR (CaF2 windows, CH_3CN, 23 °C): ν(NO) = 1734 cm^{-1} (s). UV-vis absorption spectrum [CH_3CN, λ_{max}, nm

(ε_M, M^{-1} cm^{-1})]: 417 (5800), 617 (545), 750 (325). Cyclic voltammetry ($E_{1/2}$): **[FePtFe]$^{2+}$** + e^- → **[FePtFe]$^+$** (-0.76 V), **[FePtFe]$^+$** + e^- → **[FePtFe]^0** (-0.97 V). ESI-MS positive mode: $[M]^{2+}$ = 401.50 m/z. Anal. Calcd for $H_{36}C_{18}O_2N_6S_4Fe_2B_2F_8Pt$: H, 3.71; C, 22.13; N, 8.60; S, 13.12. Found: H, 3.93; C, 22.87; N, 8.39; S, 12.90.

X-ray crystallography. The crystal structures of **[FeMFe][BF$_4$]$_2$** (M = Ni: CCDC # 2231567, M = Pd: 2231568, M = Pt: 2231569) were measured at 110 K on a Bruker Quest X-ray (fixed-Chi geometry) diffractometer with a Mo-Iμs X-ray tube (K_α = 0.71073 Å). Integrated intensity information for each reflection was obtained by reduction of the data frames with the program APEX4,[2] including the two domains. The integration method employed a three-dimensional profiling algorithm and all data were corrected for Lorentz and polarization factors, as well as for crystal decay effects. Finally, the data for each of the three **[FeMFe][BF$_4$]** structures were merged and scaled to produce a suitable data set. The absorption correction program TWINABS[3] was employed to correct the data for absorption effects, as well as to separate files: twin4.hkl, containing non-overlapping reflections, and twin5.hkl, containing reflections only from the major component. While the former was used for structure solution, the latter was used for final least squares refinement. Using Olex2,[4] the structures of **[FeMFe][BF$_4$]$_2$** were solved with the SHELXT[5] structure solution program using Intrinsic Phasing and refined with the SHELXL[6] refinement package using Least Squares minimization. The structures of **[FeMFe]$^{2+}$** were solved and refined with two half molecules in the $P\bar{1}$ space group with Z = 2, and Z' = 2 x 0.5 which results in two independent structures with similar metrical parameters. Hydrogen atoms were placed on their parent atoms and set to idealized positions. All non-hydrogen atoms were refined with anisotropic thermal patterns. Absence of additional symmetry was confirmed by PLATON.[7]

Electrochemistry. A CHI600E electrochemical analyser from CH Instruments Inc. was used to acquire cyclic voltammetry data. An air-tight, three-electrode cell was used during measurements

which were carried out at room temperature under anaerobic conditions with CH_3CN as the solvent. A concentration of 0.1 M [$^tBu_4N$][PF_6] was used for the electrolyte, and the concentration of the analyte was 1.0 mM. The working electrode was a 0.071 cm^2 glassy carbon disk, the reference electrode was a Ag/$AgNO_3$ CH_3CN solution in a Vycor-tipped glass tube, and the counter electrode was a platinum wire. All potentials were referenced to the Fc/Fc^+ couple at 0.00 V. Care was taken to ensure that the analyte was not exposed to O_2 during the experiment, and an alumina-water slurry was used to polish the electrode as needed.

Magnetic Measurements. DC magnetic measurements were performed on freshly prepared, crushed crystalline samples of **[FeMFe]$^{2+}$**. The sample was placed in a eiscosane matrix inside and NMR tube (high quality) and measured at a temperature range from 2-300 K in an applied magnetic field of 10000 Oe on a Quantum Design SQUID, Model MPMS with a 7 Tesla magnet. To restrain the crystals, the eicosane was heated (40 °C) and homogenously dispersed throughout the sample. The NMR tube was then vacuumed sealed with a butane torch. The diamagnetic contribution from the eicosane was subtracted from the raw data. The molar paramagnetic susceptibilities ($\chi_M T$) were obtained by using Pascal's constants to subtract the diamagnetic corrections of the atoms from the experimental susceptibilities.[8] A paramagnetic (S = 1/2) impurity of 2% contribution was added to the fits of **[FeNiFe]$^{2+}$** and **[FePdFe]$^{2+}$**. Magnetic (SQUID) data was fitted using the PHI® software.[9]

CW-EPR Measurement. A Bruker (Billerica, MA) ELEXSYS E540 X-band spectrometer was used to measure continuous wave (CW) EPR of **[FePdFe]$^{2+}$** as a frozen solution (1:1 DCM/CH_3CN). The spectrometer was equipped with an ER 4116 dual mode resonator, an Oxford ESR900 cryostat, and Oxford ITC 04 temperature controller. EPR spectra were collected with microwave field polarizations (**B_1**) both perpendicular and parallel to the applied magnetic field (**B_0**) with a nominal microwave frequency of 9.65 GHz and 9.41 GHz, respectively. All spectra

were collected under non-saturating conditions with a modulating frequency of 100 kHz and a modulating amplitude of 0.9 mT. Temperature dependent measurements were obtained from 6 - 65 K using liquid helium. Simulations of EPR data were performed using the custom software package, Spincount (version 7.0.8087.17737), developed by Professor Michael Hendrich at Carnegie Mellon University.[10] Simulations are calculated from the general spin Hamiltonian shown in **Eqn (S1)**,

$$\hat{H} = D\left(\hat{S}_z^2 - S(S+1)/3\right) + E\left(\hat{S}_x^2 - \hat{S}_y^2\right) + g\mu_B \vec{B} \cdot \hat{S} \quad \textbf{Eqn (S1)}$$

where D and E are the axial and rhombic zero-field splitting (zfs) parameters and $\boldsymbol{g}$ is the g-tensor.[11]

Simulations were generated with consideration of all intensity factors, both theoretical and experimental, to allow for determination of species concentration. The only unknown factor relating the spin concentration to signal intensity was an instrumental factor that is specific to the microwave detection system. This factor was determined by a Cu(EDTA) spin standard prepared from a copper atomic absorption standard solution purchased from Sigma-Aldrich.

The energy between the ground state and the excited state (|0>, |±1>) was obtained by fitting the temperature-normalized signal intensity data (S × T) to a Boltzmann population distribution for a 2-level system, **Eqn (S2)**:

$$\boldsymbol{Intensity\ x\ T} = \frac{g_i \cdot e^{-\Delta E_i/k_b T}}{\sum_j g_j \cdot e^{-\Delta E_j/k_b T}} \quad \textbf{Eqn (S2)}$$

All simulations were calculated with consideration of all theoretical and experimental intensity factors in order to determine species concentration. An instrumental factor specific to the microwave detection system was the only unknown factor relating the spin concentration to the signal intensity. A standardized EPR sample of 1.00 mM [Cu^{2+}(EDTA)], prepared from a

calibrated Cu atomic absorption standard (Sigma Aldrich), was used to determine this instrumental factor.

Computational Methodology

Density functional theory (DFT) calculations were performed in Gaussian 16Revision B.010[12] with the TPSSTPSS[13] functional. Triple-ζ basis set 6-311++G(d,p) was used for non-metals[14-16] and the Wachters-Hay basis set under the designation 6-311++G(d,p)[17-19] and the correlation consistent basis set cc-pVTZ[20] for iron and nickel, respectively. For palladium and platinum an Effective Core Potential (ECP) and a triple-ζ quality basis set (cc-pVTZ-PP) was used for core and valence electrons, respectively.[21,22] The crystal structures of **[FeMFe]$^{2+}$** were imported to use as the starting coordinates for gas phase optimization and frequency calculations using GaussView 6.0.16.[23] All species were confirmed to be minimum energy structures by the absence of imaginary frequencies. Lower-spin BS solutions were converged by repopulation of the converged orbitals from the high-spin solutions.

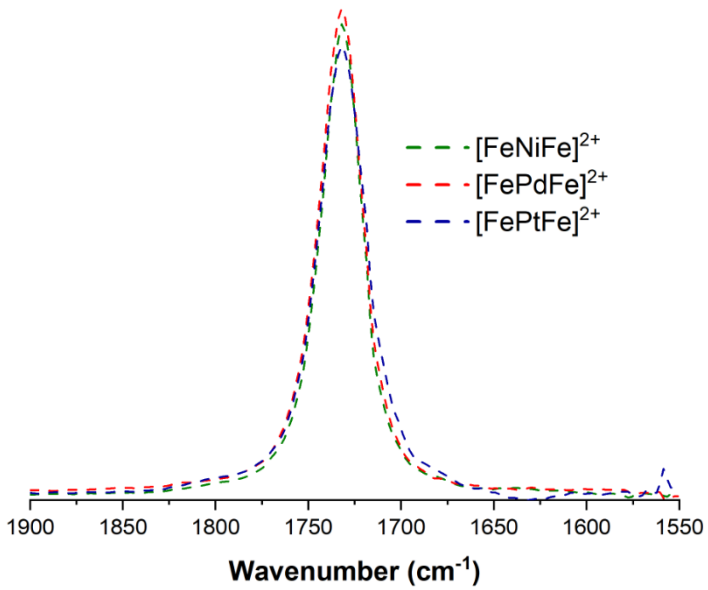

Figure S1. Infrared spectra of **[FeMFe]$^{2+}$** as its BF_4^- salts recorded in CH_3CN.

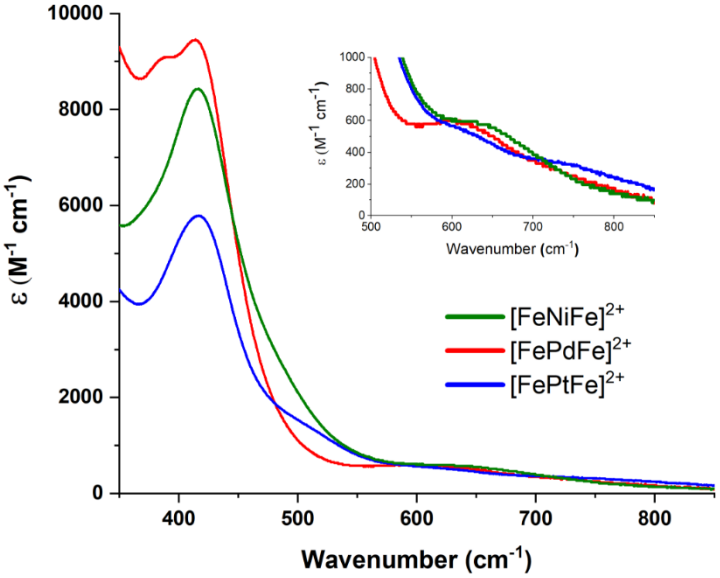

Figure S2. UV-Vis spectra of **[FeMFe][BF$_4$]$_2$** recorded in CH_3CN. Inset: expanded spectra in the visible region.

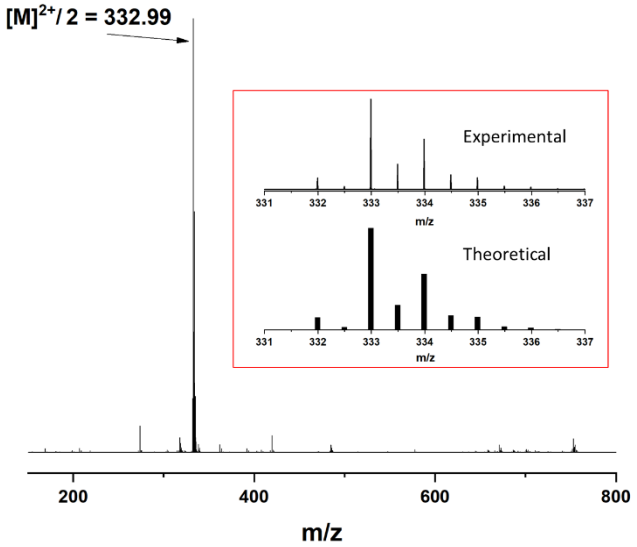

Figure S3. Positive-ion ESI-MS data of **[FeNiFe]**$^{2+}$ with isotopic bundle (inset) recorded in CH_3CN.

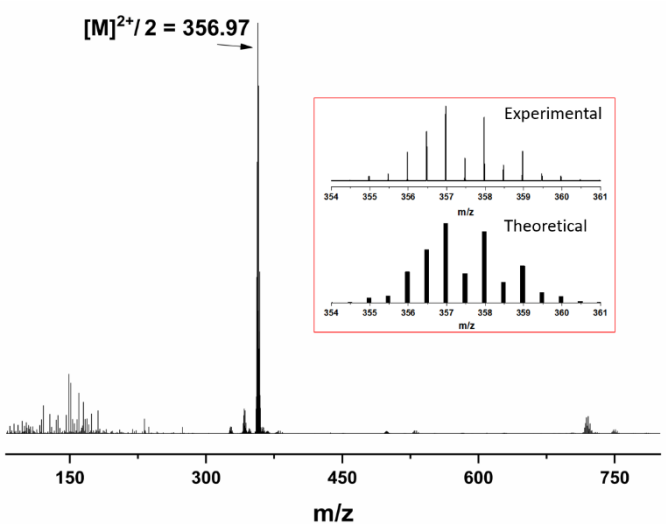

Figure S4. Positive-ion ESI-MS data of **[FePdFe]**$^{2+}$ with isotopic bundle (inset) recorded in CH_3CN.

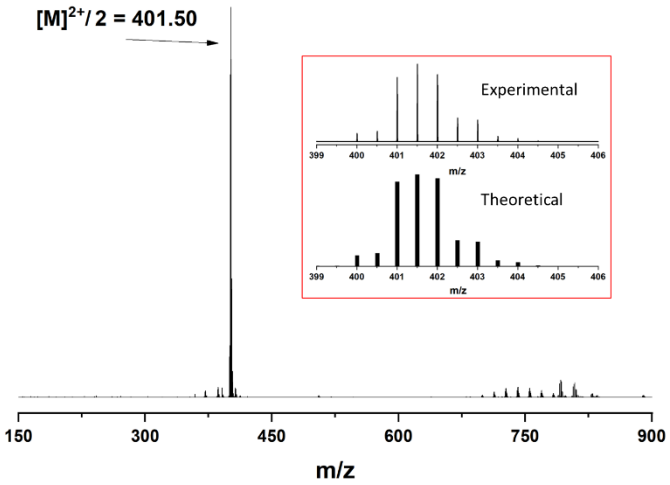

Figure S5. Positive-ion ESI-MS data of **[FePtFe]**$^{2+}$ with isotopic bundle (inset) recorded in CH_3CN.

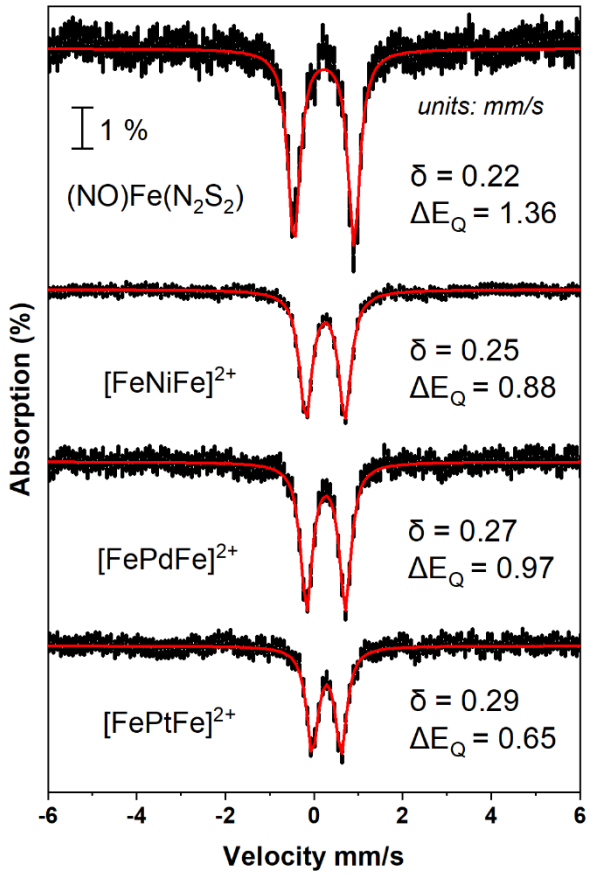

Figure S6. T=4.2 K, zero field ^{57}Fe Mössbauer spectra of samples. The black lines represent samples of **(NO)Fe(N_2S_2)** [(N_2S_2) = bme-dach], **[FeNiFe][BF_4]$_2$**, **[FePdFe][BF_4]$_2$**, and **[FePtFe][BF_4]$_2$**.Red lines show spectral simulations for the spectra with parameters shown in **Table S1**.

Table S1. Simulation parameters of Mössbauer spectra shown in **Figure S6**.

Sample	**(NO)Fe(N_2S_2)**	**[FeNiFe][BF_4]$_2$**	**[FePdFe][BF_4]$_2$**	**[FePtFe][BF_4]$_2$**
δ(mm/s)	0.22	0.25	0.27	0.29
ΔE_Q(mm/s)	1.36	0.88	0.97	0.65
Γ(mm/s)	0.32	0.34	0.31	0.31

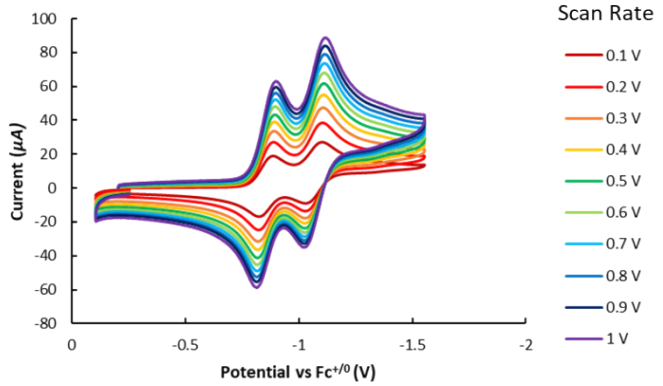

Figure S7. Scan rate dependence for the two reversible redox couples of **[FeNiFe][BF$_4$]$_2$** in CH_3CN.

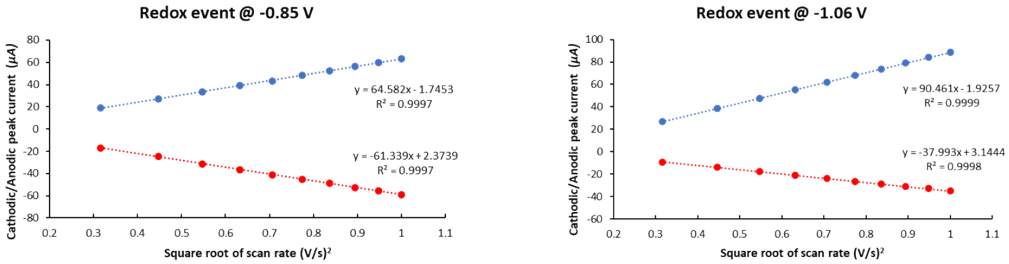

Figure S8. Plots of the cathodic/anodic peak current versus the square root of scan rate for **[FeNiFe][BF$_4$]$_2$** at different scan rates for the redox event at – 0.85 V (left) and at – 1.06 V (right).

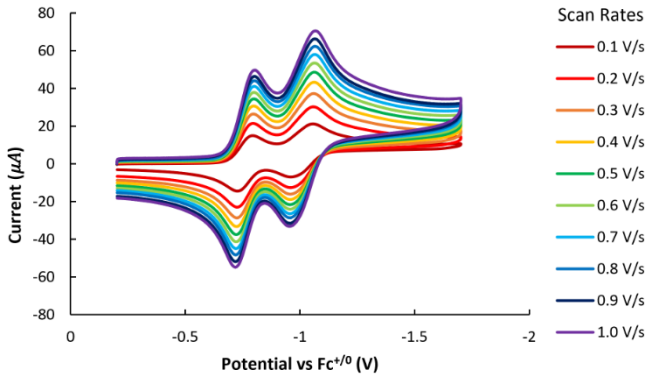

Figure S9. Scan rate dependence for the two reversible redox couples of **[FePdFe][BF$_4$]$_2$** in CH_3CN.

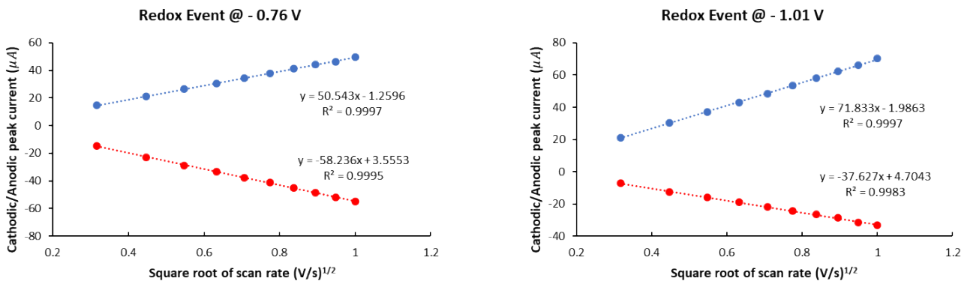

Figure S10. Plots of the cathodic/anodic peak current versus the square root of scan rate for **[FePdFe][BF$_4$]$_2$** at different scan rates for the redox event at – 0.76 V (left) and at – 1.01 V (right).

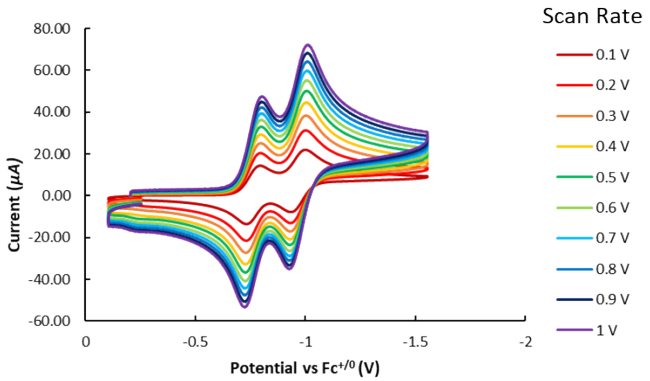

Figure S11. Scan rate dependence for the two reversible redox couples of **[FePtFe][BF$_4$]$_2$** in CH_3CN.

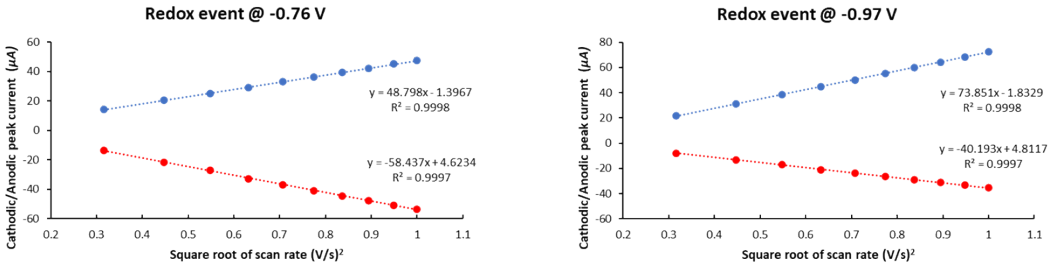

Figure S12. Plots of the cathodic/anodic peak current versus the square root of scan rate for **[FePtFe][BF$_4$]$_2$** at different scan rates for the redox event at – 0.76 V (left) and at – 0.97 V (right).

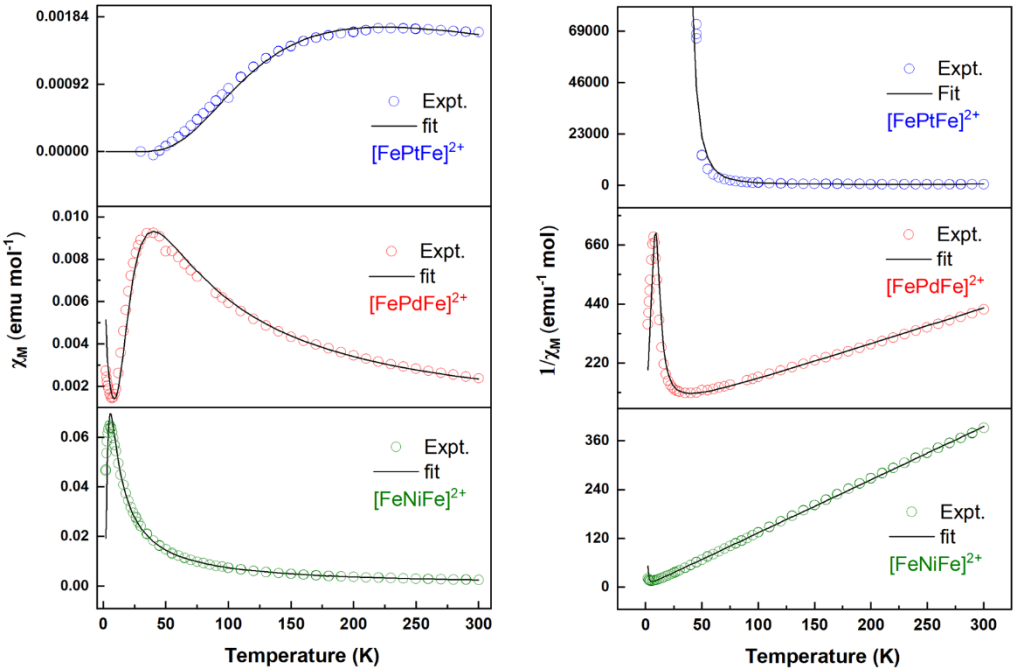

Figure S13. χ_M vs. T (left) and $1/\chi_M$ vs. T (right) plots of **[FeMFe][BF$_4$]$_2$** collected between 2 and 300 K with a 1 T field (circles: raw data, black line: fit).

Table S2. Crystal data and structure refinement for **[FeMFe][BF_4]$_2$.**

M =	Ni	Pd	Pt
Identification code	FeNiFe_073122_0m_4	FePdFe_2_0m_4	MQ_Q_FePtFe_107B2_0m_4
Empirical formula	$C_{22}H_{42}B_2F_8Fe_2N_8NiO_2S_4$	$C_{22}H_{42}B_2F_8Fe_2N_8O_2PdS_4$	$C_{22}H_{42}B_2F_8Fe_2N_8O_2PtS_4$
Formula weight	922.90	970.59	1059.28
Temperature/K	110.00	110.00	120.00
Crystal system	triclinic	triclinic	triclinic
Space group	P-1	P-1	P-1
a/Å	7.7964(6)	7.8814(4)	7.9001(10)
b/Å	11.2004(8)	11.2000(5)	11.1920(13)
c/Å	20.4101(14)	20.5038(9)	20.377(2)
α/°	85.406(2)	85.3290(10)	85.430(3)
β/°	89.714(2)	89.1940(10)	89.241(3)
γ/°	82.273(2)	82.4020(10)	82.767(2)
Volume/Å^3	1760.4(2)	1788.05(14)	1781.7(4)
Z	2	2	2
ρ_{calc}g/cm^3	1.741	1.803	1.974
μ/mm^{-1}	1.659	1.610	5.033
F(000)	944.0	980.0	1044.0
Crystal size/mm^3	0.142 × 0.023 × 0.015	0.3 × 0.3 × 0.3	0.3 × 0.3 × 0.3
Radiation	MoKα (λ = 0.71073)	MoKα (λ = 0.71073)	MoKα (λ = 0.71073)
2Θ range for data collection/°	3.682 to 50.14	3.68 to 60.124	3.68 to 58.42
Index ranges	-9 ≤ h ≤ 9, -13 ≤ k ≤ 13, 0 ≤ l ≤ 24	-11 ≤ h ≤ 11, -15 ≤ k ≤ 15, 0 ≤ l ≤ 28	-10 ≤ h ≤ 10, -15 ≤ k ≤ 15, 0 ≤ l ≤ 27
Reflections collected	5987	9317	8623
Independent reflections	5987 [R_{int} = ?, R_{sigma} = 0.0757]	9317 [R_{int} = ?, R_{sigma} = 0.0434]	8623 [R_{int} = 0.0499, R_{sigma} = 0.0572]
Data/restraints/parameters	5987/3/430	9317/0/448	8623/0/448
Goodness-of-fit on F^2	1.139	1.172	1.024
Final R indexes [I>=2σ (I)]	R_1 = 0.0675[a], wR_2 = 0.1588[b]	R_1 = 0.0422[a], wR_2 = 0.1079[b]	R_1 = 0.0355[a], wR_2 = 0.0781[b]
Final R indexes [all data]	R_1 = 0.0906[a], wR_2 = 0.1709[b]	R_1 = 0.0529[a], wR_2 = 0.1219[b]	R_1 = 0.0439[a], wR_2 = 0.0806[b]
Largest diff. peak/hole / e Å^{-3}	0.65/-0.73	0.70/-0.81	1.64/-1.53

[a]$R_1=\Sigma(||F_o|-|F_c||)/\Sigma|F_o|$. [b]$wR_2=[\Sigma[w(F_o^2-F_c^2)^2]/\Sigma[w(F_o^2)^2]]^{1/2}$, $w=1/[\sigma^2(F_o^2)+(ap)^2+bp]$, where $p=[\max(F_o^2, 0)+2F_c^2]/3$.

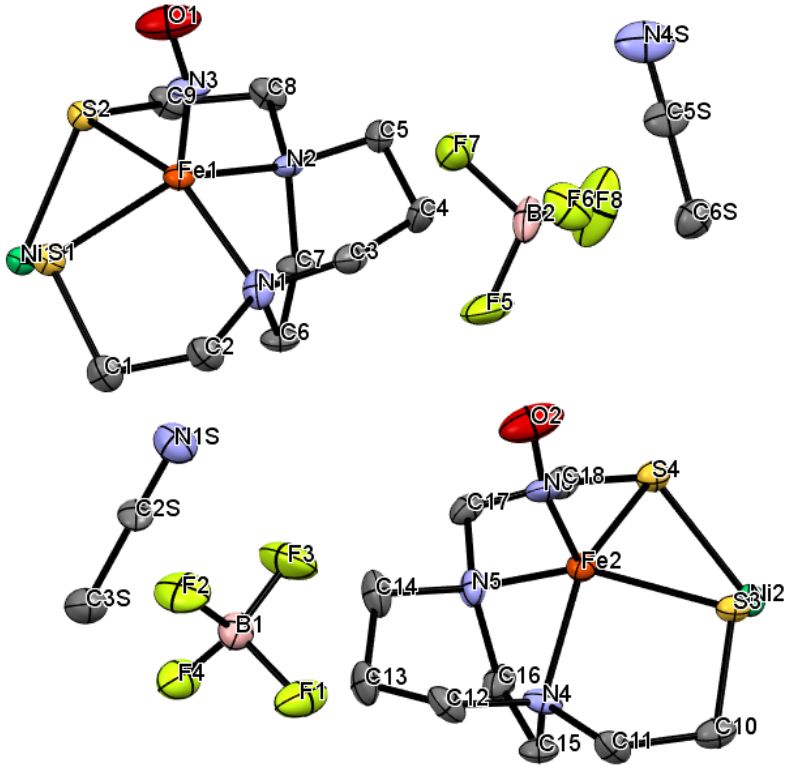

Figure S14. Asymmetric unit along the *a* axis of the **[FeNiFe][BF$_4$]$_2$** showing two half molecules. Hydrogen atoms omitted for clarity; thermal ellipsoids at 50 % probability.

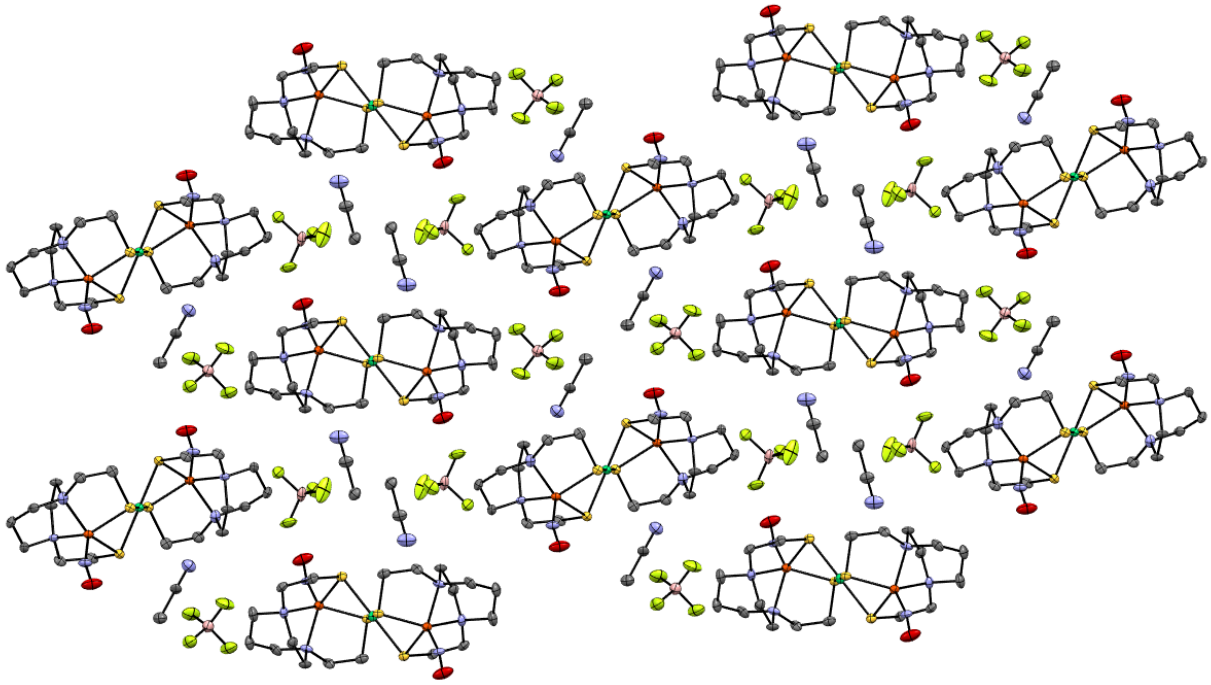

Figure S15. X-ray crystal packing of **[FeNiFe][BF$_4$]$_2$** along the *a* axis.

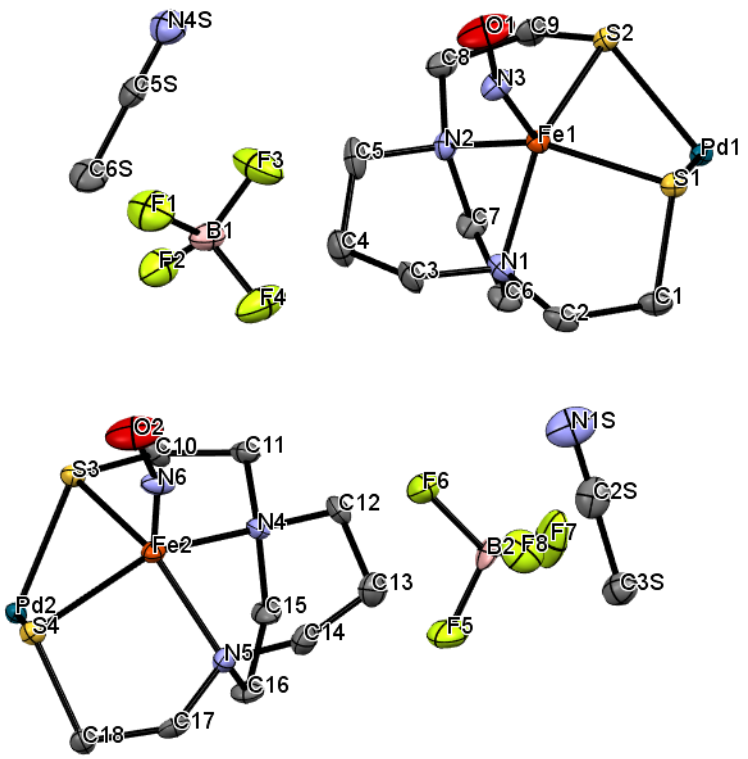

Figure S16. Asymmetric unit along the *a* axis of the **[FePdFe][BF$_4$]$_2$** showing two half molecules. Hydrogen atoms omitted for clarity; thermal ellipsoids at 50 % probability.

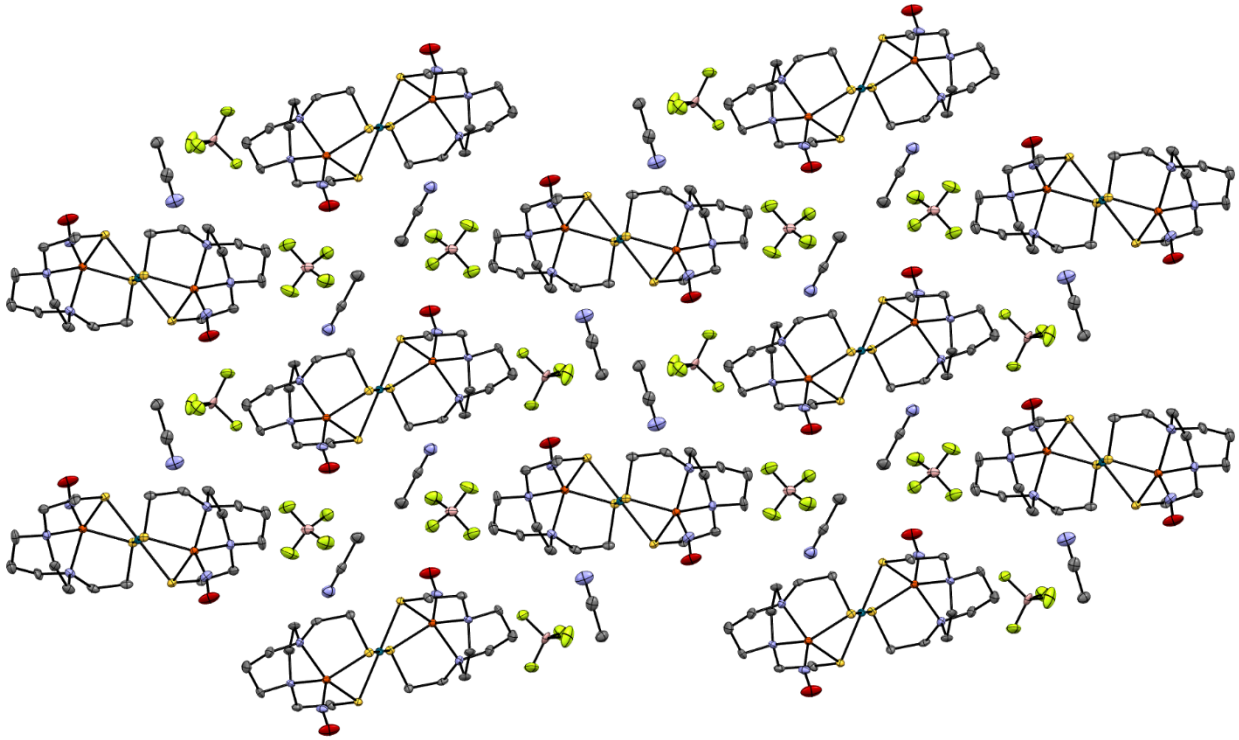

Figure S17. X-ray crystal packing of **[FePdFe][BF$_4$]$_2$** along the *a* axis.

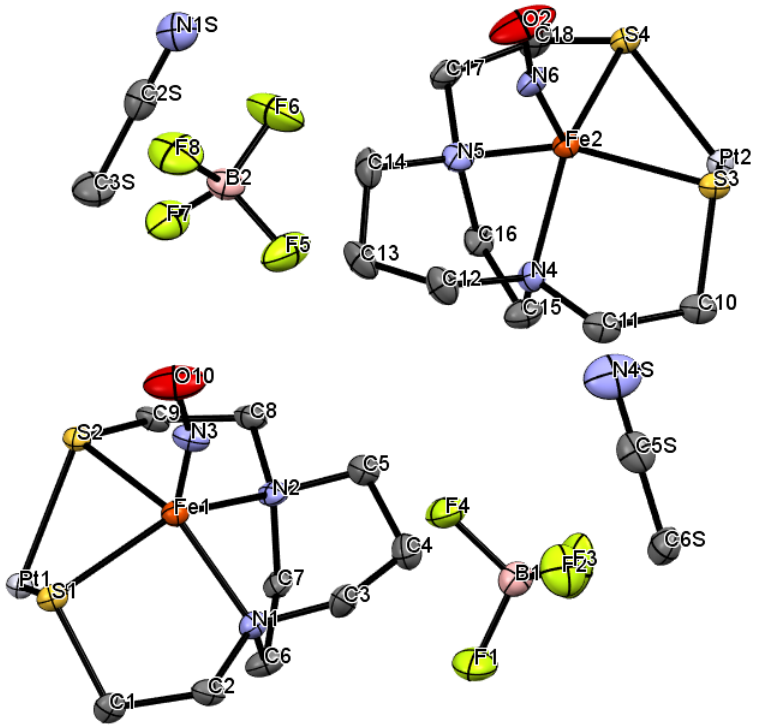

Figure S18. Asymmetric unit along the *a* axis of the **[FePtFe][BF$_4$]$_2$** showing two half molecules. Hydrogen atoms omitted for clarity; thermal ellipsoids at 50 % probability.

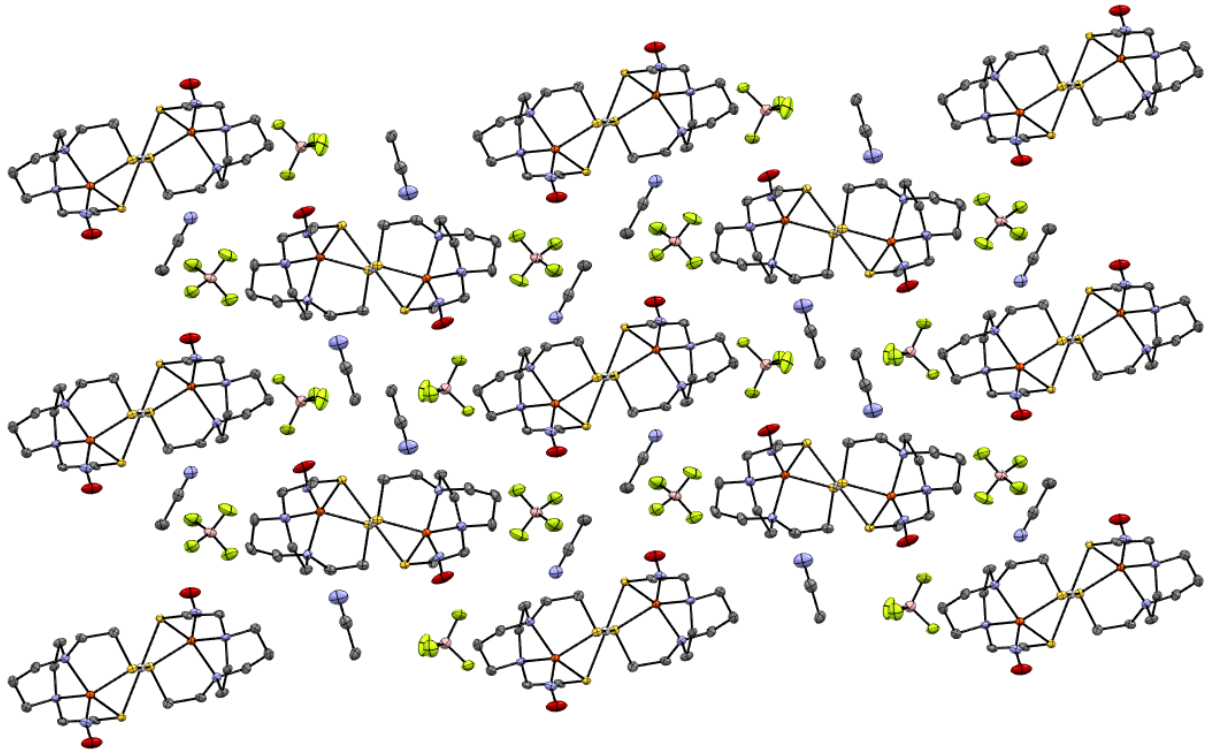

Figure S19. X-ray crystal packing of **[FePtFe][BF$_4$]$_2$** along the *a* axis.

Table S3. Selected Bond Lengths for **[FeNiFe][BF$_4$]$_2$.**

Atom	Atom	Length/Å	Atom	Atom	Length/Å
Ni1	Fe1[1]	2.9558(17)	Ni2	Fe2[2]	2.9480(18)
Ni1	Fe1	2.9558(17)	Ni2	Fe2	2.9481(18)
Ni1	S1[1]	2.204(3)	Ni2	S3	2.206(3)
Ni1	S1	2.204(3)	Ni2	S3[2]	2.206(3)
Ni1	S2[1]	2.199(3)	Ni2	S4	2.202(3)
Ni1	S2	2.199(3)	Ni2	S4[2]	2.202(3)
Fe1	S1	2.234(3)	Fe2	S3	2.241(3)
Fe1	S2	2.223(3)	Fe2	S4	2.227(4)
Fe1	N1	2.002(11)	Fe2	N4	2.009(10)
Fe1	N2	2.011(10)	Fe2	N5	2.012(10)
Fe1	N3	1.687(10)	Fe2	N6	1.671(11)
S1	C1	1.841(13)	S3	C10	1.824(13)
S2	C9	1.832(12)	S4	C18	1.835(12)
O1	N3	1.161(13)	O2	N6	1.169(14)

[1]2-X,1-Y,-Z; [2]1-X,-Y,1-Z

Table S4. Selected Bond Lengths for **[FePdFe][BF$_4$]$_2$.**

Atom	Atom	Length/Å	Atom	Atom	Length/Å
Pd1	Fe1	3.0030(8)	Pd2	Fe2[2]	3.0084(8)
Pd1	Fe1[1]	3.0030(8)	Pd2	Fe2	3.0084(8)
Pd1	S1[1]	2.3173(14)	Pd2	S3[2]	2.3177(14)
Pd1	S1	2.3173(14)	Pd2	S3	2.3177(14)
Pd1	S2[1]	2.3266(15)	Pd2	S4	2.3197(14)
Pd1	S2	2.3265(15)	Pd2	S4[2]	2.3197(14)
Fe1	S1	2.2602(17)	Fe2	S3	2.2403(17)
Fe1	S2	2.2416(17)	Fe2	S4	2.2528(17)
Fe1	N1	2.017(5)	Fe2	N4	2.017(5)
Fe1	N2	2.018(5)	Fe2	N5	2.020(5)
Fe1	N3	1.691(5)	Fe2	N6	1.697(5)
S1	C1	1.841(6)	S3	C10	1.842(6)
S2	C9	1.843(7)	S4	C18	1.851(6)
O1	N3	1.160(7)	O2	N6	1.159(7)

[1]2-X,1-Y,-Z; [2]1-X,-Y,1-Z

Table S5. Selected Bond Lengths for **[FePtFe][BF$_4$]$_2$.**

Atom	Atom	Length/Å	Atom	Atom	Length/Å
Pt1	Fe1	2.9707(9)	Pt2	Fe2	2.9678(9)
Pt1	Fe1[1]	2.9707(9)	Pt2	Fe2[2]	2.9677(9)
Pt1	S1	2.3156(16)	Pt2	S3[2]	2.3127(16)
Pt1	S1[1]	2.3156(16)	Pt2	S3	2.3127(16)
Pt1	S2[1]	2.3185(15)	Pt2	S4[2]	2.3242(16)
Pt1	S2	2.3185(15)	Pt2	S4	2.3242(16)
Fe1	S1	2.2638(19)	Fe2	S3	2.268(2)
Fe1	S2	2.2474(18)	Fe2	S4	2.2480(18)
Fe1	N1	2.010(5)	Fe2	N4	2.009(6)
Fe1	N2	2.009(6)	Fe2	N5	2.013(6)
Fe1	N3	1.689(5)	Fe2	N6	1.686(5)
S1	C1	1.829(6)	S3	C10	1.835(7)
S2	C9	1.837(6)	S4	C18	1.836(7)
O10	N3	1.156(7)	O2	N6	1.159(7)

[1]2-X,1-Y,-Z; [2]1-X,-Y,1-Z

Table 6. Bond Angles for **[FeNiFe][BF4]$_2$.**

Atom	Atom	Atom	Angle/°	Atom	Atom	Atom	Angle/°
Fe1	Ni1	Fe1[1]	180.0	S4[2]	Ni2	Fe2	131.37(9)
S1	Ni1	Fe1[1]	131.33(8)	S4[2]	Ni2	Fe2[2]	48.63(9)
S1	Ni1	Fe1	48.67(8)	S4	Ni2	Fe2	48.63(9)
S1[1]	Ni1	Fe1[1]	48.67(8)	S4	Ni2	S3	83.89(11)
S1[1]	Ni1	Fe1	131.33(8)	S4[2]	Ni2	S3[2]	83.89(11)
S1[1]	Ni1	S1	180.0	S4	Ni2	S3[2]	96.11(11)
S2[1]	Ni1	Fe1[1]	48.41(8)	S4[2]	Ni2	S3	96.11(11)
S2[1]	Ni1	Fe1	131.59(8)	S4[2]	Ni2	S4	180.00(16)
S2	Ni1	Fe1[1]	131.59(8)	S3	Fe2	Ni2	47.96(9)
S2	Ni1	Fe1	48.41(8)	S4	Fe2	Ni2	47.90(9)
S2[1]	Ni1	S1	95.16(11)	S4	Fe2	S3	82.50(13)
S2	Ni1	S1	84.84(11)	N4	Fe2	Ni2	102.3(3)
S2	Ni1	S1[1]	95.16(11)	N4	Fe2	S3	87.8(3)
S2[1]	Ni1	S1[1]	84.84(11)	N4	Fe2	S4	145.1(3)
S2	Ni1	S2[1]	180.0	N4	Fe2	N5	79.8(4)
S1	Fe1	Ni1	47.80(8)	N5	Fe2	Ni2	102.0(3)
S2	Fe1	Ni1	47.71(9)	N5	Fe2	S3	144.1(3)
S2	Fe1	S1	83.57(12)	N5	Fe2	S4	88.7(3)
N1	Fe1	Ni1	104.8(3)	N6	Fe2	Ni2	139.2(4)
N1	Fe1	S1	88.5(3)	N6	Fe2	S3	108.4(4)
N1	Fe1	S2	146.5(3)	N6	Fe2	S4	104.7(4)
N1	Fe1	N2	80.0(4)	N6	Fe2	N4	110.1(5)
N2	Fe1	Ni1	104.2(3)	N6	Fe2	N5	107.5(5)
N2	Fe1	S1	145.8(3)	Ni2	S3	Fe2	83.07(11)
N2	Fe1	S2	88.5(3)	C10	S3	Ni2	109.7(4)
N3	Fe1	Ni1	135.4(4)	C10	S3	Fe2	100.2(4)
N3	Fe1	S1	105.8(4)	Ni2	S4	Fe2	83.46(12)
N3	Fe1	S2	103.4(4)	C18	S4	Ni2	109.2(4)
N3	Fe1	N1	110.1(5)	C18	S4	Fe2	99.5(4)
N3	Fe1	N2	108.4(5)	F2	B1	F1	109.4(12)
Ni1	S1	Fe1	83.53(11)	F2	B1	F4	111.4(12)
C1	S1	Ni1	109.8(4)	F3	B1	F1	107.6(12)
C1	S1	Fe1	99.7(4)	F3	B1	F2	109.8(13)
Ni1	S2	Fe1	83.88(11)	F3	B1	F4	111.5(13)
C9	S2	Ni1	109.3(4)	F4	B1	F1	107.1(12)
C9	S2	Fe1	99.9(4)	F5	B2	F6	108.6(13)
C2	N1	Fe1	111.8(8)	F5	B2	F7	108.1(12)
C3	N1	Fe1	112.0(8)	F5	B2	F8	112.7(13)
C3	N1	C2	107.8(10)	F6	B2	F7	108.8(12)
C6	N1	Fe1	103.2(7)	F8	B2	F6	109.6(12)
C6	N1	C2	111.9(10)	F8	B2	F7	109.0(14)
C6	N1	C3	110.2(10)	N1S	C2S	C3S	179.5(16)
C5	N2	Fe1	111.3(8)	C11	N4	Fe2	112.3(7)
C5	N2	C7	110.7(9)	C11	N4	C12	107.3(9)
C7	N2	Fe1	102.5(7)	C11	N4	C15	112.4(10)
C8	N2	Fe1	112.5(7)	C12	N4	Fe2	112.1(8)
C8	N2	C5	107.8(9)	C15	N4	Fe2	102.4(7)
C8	N2	C7	112.0(9)	C15	N4	C12	110.4(10)
O1	N3	Fe1	159.8(11)	N4S	C5S	C6S	179.0(17)
C2	C1	S1	108.8(9)	C14	N5	Fe2	113.0(8)
C1	C2	N1	112.8(10)	C16	N5	Fe2	101.7(7)
N1	C3	C4	112.4(10)	C16	N5	C14	111.1(10)
C3	C4	C5	114.8(10)	C17	N5	Fe2	111.6(8)
N2	C5	C4	112.8(10)	C17	N5	C14	107.1(10)
N1	C6	C7	110.8(10)	C17	N5	C16	112.4(9)
N2	C7	C6	110.1(10)	O2	N6	Fe2	165.5(11)
N2	C8	C9	112.3(10)	C11	C10	S3	109.3(9)
C8	C9	S2	109.7(8)	N4	C11	C10	112.4(10)
Fe2[2]	Ni2	Fe2	180.0	N4	C12	C13	112.7(10)
S3	Ni2	Fe2	48.98(9)	C14	C13	C12	115.3(11)
S3[2]	Ni2	Fe2[2]	48.98(9)	C13	C14	N5	112.6(11)
S3	Ni2	Fe2[2]	131.02(9)	N4	C15	C16	110.7(10)
S3[2]	Ni2	Fe2	131.02(9)	N5	C16	C15	110.0(10)
S3[2]	Ni2	S3	180.0	N5	C17	C18	112.9(10)
S4	Ni2	Fe2[2]	131.37(9)	C17	C18	S4	110.5(9)

[1]2-X,1-Y,-Z; [2]1-X,-Y,1-Z

Table 7. Bond Angles for **[FePdFe][BF4]$_2$.**

Atom	Atom	Atom	Angle/°	Atom	Atom	Atom	Angle/°
Fe1[1]	Pd1	Fe1	180.0	S3[2]	Pd2	S4	97.08(5)
S1	Pd1	Fe1	48.18(4)	S3[2]	Pd2	S4[2]	82.92(5)
S1[1]	Pd1	Fe1	131.82(4)	S3	Pd2	S4	82.92(5)
S1	Pd1	Fe1[1]	131.82(4)	S4	Pd2	Fe2[2]	132.09(4)
S1[1]	Pd1	Fe1[1]	48.18(4)	S4	Pd2	Fe2	47.91(4)
S1	Pd1	S1[1]	180.0	S4[2]	Pd2	Fe2[2]	47.91(4)
S1	Pd1	S2[1]	98.09(5)	S4[2]	Pd2	Fe2	132.09(4)
S1[1]	Pd1	S2	98.09(5)	S4[2]	Pd2	S4	180.0
S1	Pd1	S2	81.91(5)	S3	Fe2	Pd2	49.82(4)
S1[1]	Pd1	S2[1]	81.91(5)	S3	Fe2	S4	86.21(6)
S2[1]	Pd1	Fe1[1]	47.69(4)	S4	Fe2	Pd2	49.82(4)
S2	Pd1	Fe1[1]	132.31(4)	N4	Fe2	Pd2	103.80(16)
S2[1]	Pd1	Fe1	132.31(4)	N4	Fe2	S3	88.15(16)
S2	Pd1	Fe1	47.69(4)	N4	Fe2	S4	147.17(15)
S2	Pd1	S2[1]	180.0	N4	Fe2	N5	80.2(2)
S1	Fe1	Pd1	49.83(4)	N5	Fe2	Pd2	104.45(15)
S2	Fe1	Pd1	50.13(4)	N5	Fe2	S3	148.23(16)
S2	Fe1	S1	85.09(6)	N5	Fe2	S4	87.87(15)
N1	Fe1	Pd1	102.32(15)	N6	Fe2	Pd2	136.5(2)
N1	Fe1	S1	87.58(16)	N6	Fe2	S3	102.66(18)
N1	Fe1	S2	147.27(16)	N6	Fe2	S4	104.3(2)
N1	Fe1	N2	80.1(2)	N6	Fe2	N4	108.4(2)
N2	Fe1	Pd1	101.40(15)	N6	Fe2	N5	109.0(2)
N2	Fe1	S1	145.42(16)	Fe2	S3	Pd2	82.58(5)
N2	Fe1	S2	88.10(16)	C10	S3	Pd2	106.9(2)
N3	Fe1	Pd1	140.0(2)	C10	S3	Fe2	99.8(2)
N3	Fe1	S1	106.91(19)	Fe2	S4	Pd2	82.27(5)
N3	Fe1	S2	103.4(2)	C18	S4	Pd2	107.7(2)
N3	Fe1	N1	109.3(2)	C18	S4	Fe2	99.9(2)
N3	Fe1	N2	107.7(2)	C11	N4	Fe2	112.9(4)
Fe1	S1	Pd1	81.99(5)	C11	N4	C12	107.0(5)
C1	S1	Pd1	107.9(2)	C11	N4	C15	112.2(5)
C1	S1	Fe1	99.7(2)	C12	N4	Fe2	111.8(4)
Fe1	S2	Pd1	82.18(5)	C15	N4	Fe2	101.9(4)
C9	S2	Pd1	106.9(2)	C15	N4	C12	111.2(5)
C9	S2	Fe1	99.7(2)	C14	N5	Fe2	112.0(4)
C2	N1	Fe1	112.2(4)	C14	N5	C16	111.2(5)
C2	N1	C3	107.1(5)	C14	N5	C17	107.3(5)
C2	N1	C6	112.2(5)	C16	N5	Fe2	102.1(4)
C3	N1	Fe1	112.1(4)	C17	N5	Fe2	112.6(4)
C3	N1	C6	111.4(5)	C17	N5	C16	111.7(5)
C6	N1	Fe1	101.9(4)	O2	N6	Fe2	158.6(6)
C5	N2	Fe1	112.1(4)	C11	C10	S3	108.8(4)
C7	N2	Fe1	101.9(4)	N4	C11	C10	112.2(5)
C7	N2	C5	110.6(5)	N4	C12	C13	113.2(5)
C8	N2	Fe1	113.1(4)	C12	C13	C14	115.0(6)
C8	N2	C5	106.5(5)	N5	C14	C13	113.1(6)
C8	N2	C7	112.7(5)	N4	C15	C16	110.8(5)
O1	N3	Fe1	162.7(6)	N5	C16	C15	110.2(5)
C2	C1	S1	108.9(4)	N5	C17	C18	112.6(5)
N1	C2	C1	112.9(5)	C17	C18	S4	108.0(4)
N1	C3	C4	111.8(6)	F2	B1	F1	110.1(6)
C5	C4	C3	114.6(6)	F2	B1	F3	111.2(6)
C4	C5	N2	113.2(6)	F2	B1	F4	108.9(6)
N1	C6	C7	109.9(5)	F3	B1	F1	108.3(6)
N2	C7	C6	110.9(5)	F3	B1	F4	109.1(7)
N2	C8	C9	112.5(5)	F4	B1	F1	109.2(6)
C8	C9	S2	110.3(4)	F5	B2	F6	108.1(6)
Fe2	Pd2	Fe2[2]	180.0	F7	B2	F5	110.0(6)
S3	Pd2	Fe2	47.60(4)	F7	B2	F6	109.0(6)
S3[2]	Pd2	Fe2	132.40(4)	F7	B2	F8	110.6(6)
S3	Pd2	Fe2[2]	132.40(4)	F8	B2	F5	109.5(6)
S3[2]	Pd2	Fe2[2]	47.60(4)	F8	B2	F6	109.6(6)
S3[2]	Pd2	S3	180.0	N1S	C2S	C3S	179.2(9)
S3	Pd2	S4[2]	97.08(5)	N4S	C5S	C6S	179.4(8)

[1]2-X,1-Y,2-Z; [2]1-X,-Y,1-Z

Table 8. Bond Angles for **[FePtFe][BF4]$_2$.**

Atom	Atom	Atom	Angle/°	Atom	Atom	Atom	Angle/°
Fe1[1]	Pt1	Fe1	180.0	S3[2]	Pt2	S4[2]	82.36(6)
S1	Pt1	Fe1	48.80(4)	S3[2]	Pt2	S4	97.64(6)
S1[1]	Pt1	Fe1[1]	48.80(4)	S3	Pt2	S4[2]	97.64(6)
S1[1]	Pt1	Fe1	131.20(4)	S4[2]	Pt2	Fe2	131.58(4)
S1	Pt1	Fe1[1]	131.20(4)	S4	Pt2	Fe2[2]	131.58(4)
S1[1]	Pt1	S1	180.0	S4[2]	Pt2	Fe2[2]	48.42(4)
S1[1]	Pt1	S2	96.61(5)	S4	Pt2	Fe2	48.42(4)
S1	Pt1	S2	83.39(5)	S4	Pt2	S4[2]	180.00(7)
S1	Pt1	S2[1]	96.61(5)	S3	Fe2	Pt2	50.28(4)
S1[1]	Pt1	S2[1]	83.39(5)	S4	Fe2	Pt2	50.66(4)
S2[1]	Pt1	Fe1	131.62(4)	S4	Fe2	S3	85.07(7)
S2	Pt1	Fe1[1]	131.62(4)	N4	Fe2	Pt2	101.88(15)
S2	Pt1	Fe1	48.38(4)	N4	Fe2	S3	88.11(16)
S2[1]	Pt1	Fe1[1]	48.38(4)	N4	Fe2	S4	147.39(16)
S2[1]	Pt1	S2	180.00(7)	N4	Fe2	N5	79.2(2)
S1	Fe1	Pt1	50.32(4)	N5	Fe2	Pt2	101.03(18)
S2	Fe1	Pt1	50.46(4)	N5	Fe2	S3	145.58(18)
S2	Fe1	S1	86.20(7)	N5	Fe2	S4	88.64(18)
N1	Fe1	Pt1	103.58(15)	N6	Fe2	Pt2	141.1(2)
N1	Fe1	S1	87.97(16)	N6	Fe2	S3	107.19(19)
N1	Fe1	S2	148.33(16)	N6	Fe2	S4	103.3(2)
N2	Fe1	Pt1	102.95(18)	N6	Fe2	N4	109.2(2)
N2	Fe1	S1	147.12(17)	N6	Fe2	N5	107.2(3)
N2	Fe1	S2	88.31(18)	Fe2	S3	Pt2	80.75(6)
N2	Fe1	N1	80.0(2)	C10	S3	Pt2	107.1(2)
N3	Fe1	Pt1	137.7(2)	C10	S3	Fe2	99.1(2)
N3	Fe1	S1	104.4(2)	Fe2	S4	Pt2	80.93(5)
N3	Fe1	S2	102.4(2)	C18	S4	Pt2	105.8(2)
N3	Fe1	N1	109.2(3)	C18	S4	Fe2	99.5(2)
N3	Fe1	N2	108.4(3)	C11	N4	Fe2	112.4(4)
Fe1	S1	Pt1	80.88(6)	C11	N4	C12	107.0(5)
C1	S1	Pt1	106.9(2)	C12	N4	Fe2	112.1(4)
C1	S1	Fe1	98.8(2)	C15	N4	Fe2	102.8(4)
Fe1	S2	Pt1	81.16(5)	C15	N4	C11	111.9(5)
C9	S2	Pt1	105.7(2)	C15	N4	C12	110.6(6)
C9	S2	Fe1	99.4(2)	C14	N5	Fe2	113.0(4)
C2	N1	Fe1	112.5(4)	C16	N5	Fe2	103.4(4)
C2	N1	C6	112.2(5)	C16	N5	C14	110.2(6)
C3	N1	Fe1	112.1(4)	C16	N5	C17	112.1(5)
C3	N1	C2	107.1(5)	C17	N5	Fe2	112.3(4)
C3	N1	C6	110.9(5)	C17	N5	C14	105.9(6)
C6	N1	Fe1	102.1(4)	O2	N6	Fe2	165.2(6)
C5	N2	Fe1	112.0(4)	C11	C10	S3	110.0(5)
C7	N2	Fe1	102.9(4)	N4	C11	C10	113.0(5)
C7	N2	C5	110.6(5)	N4	C12	C13	112.9(6)
C8	N2	Fe1	112.5(4)	C12	C13	C14	114.8(6)
C8	N2	C5	106.7(5)	C13	C14	N5	112.5(6)
C8	N2	C7	112.2(5)	N4	C15	C16	110.2(5)
O10	N3	Fe1	160.1(6)	N5	C16	C15	109.4(6)
C2	C1	S1	109.7(4)	N5	C17	C18	112.7(6)
C1	C2	N1	112.2(5)	C17	C18	S4	110.5(5)
N1	C3	C4	113.3(6)	F1	B1	F2	109.9(6)
C3	C4	C5	114.6(6)	F1	B1	F4	108.0(6)
N2	C5	C4	112.7(6)	F2	B1	F4	109.1(6)
N1	C6	C7	110.4(6)	F3	B1	F1	110.8(6)
N2	C7	C6	110.4(5)	F3	B1	F2	110.1(7)
N2	C8	C9	113.3(5)	F3	B1	F4	108.9(6)
C8	C9	S2	108.9(4)	F5	B2	F7	108.9(6)
Fe2[2]	Pt2	Fe2	180.0	F5	B2	F8	109.2(7)
S3	Pt2	Fe2	48.97(5)	F6	B2	F5	108.9(7)
S3[2]	Pt2	Fe2	131.03(5)	F6	B2	F7	110.6(7)
S3	Pt2	Fe2[2]	131.03(5)	F6	B2	F8	109.3(6)
S3[2]	Pt2	Fe2[2]	48.97(5)	F8	B2	F7	109.8(7)
S3[2]	Pt2	S3	180.0	N1S	C2S	C3S	179.7(9)
S3	Pt2	S4	82.36(6)	N4S	C5S	C6S	179.7(9)

[1]1-X,-Y,-Z; [2]-X,1-Y,1-Z

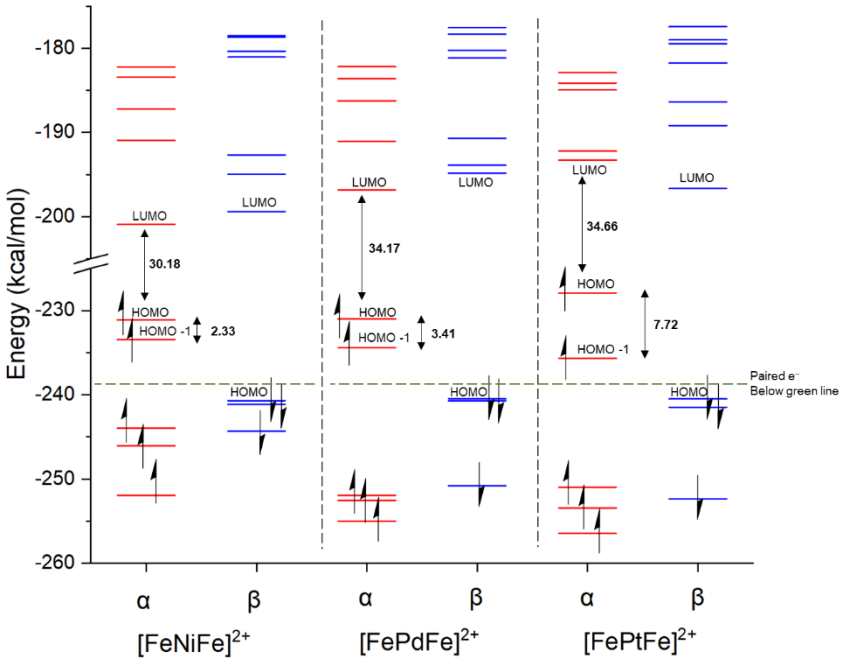

Figure S20. Alpha and Beta MO energy levels (HOMO to HOMO -4 and LUMO to LUMO +6) for the **[FeMFe]$^{2+}$** series in the triplet states.

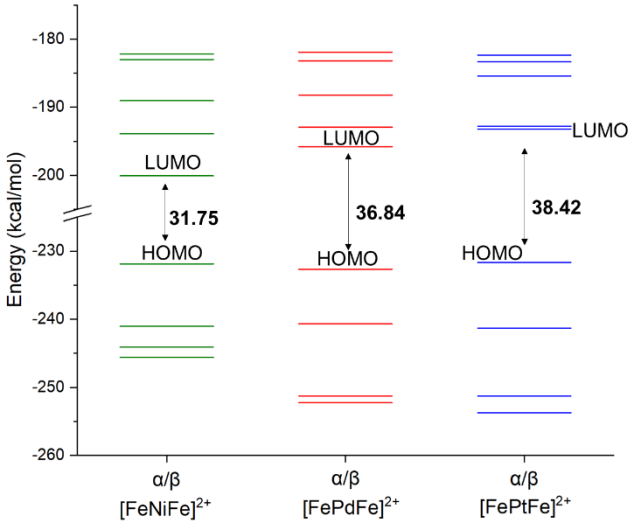

Figure S21. Alpha and Beta MO energy levels (HOMO to HOMO -3 and LUMO to LUMO +4) for the **[FeMFe]$^{2+}$** series in the BS singlet states.

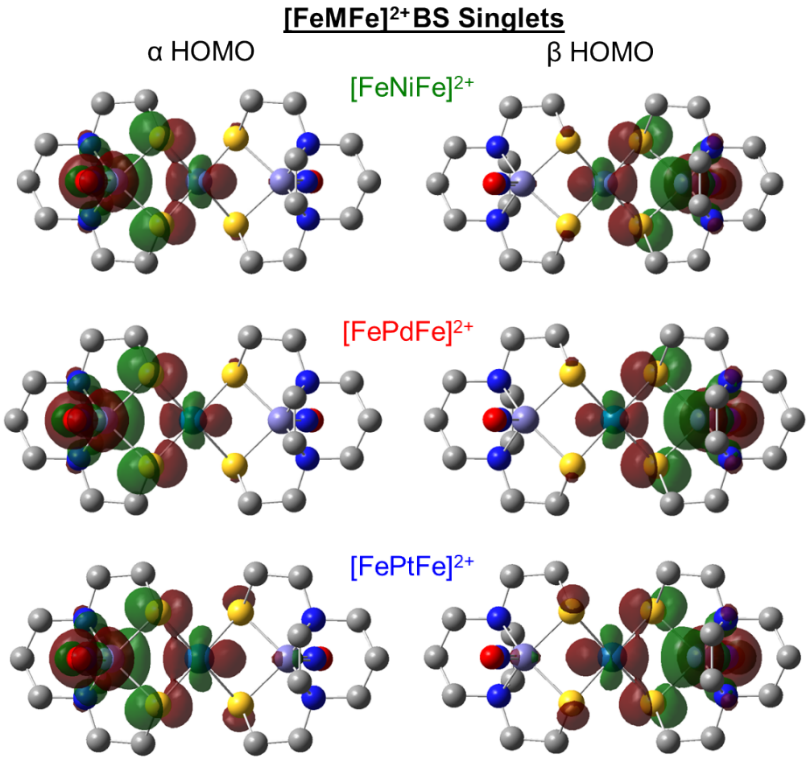

Figure S22. α HOMO and β HOMO-1 plots for the **[FeMFe]$^{2+}$** series in the BS singlet states (isovalue = 0.03).

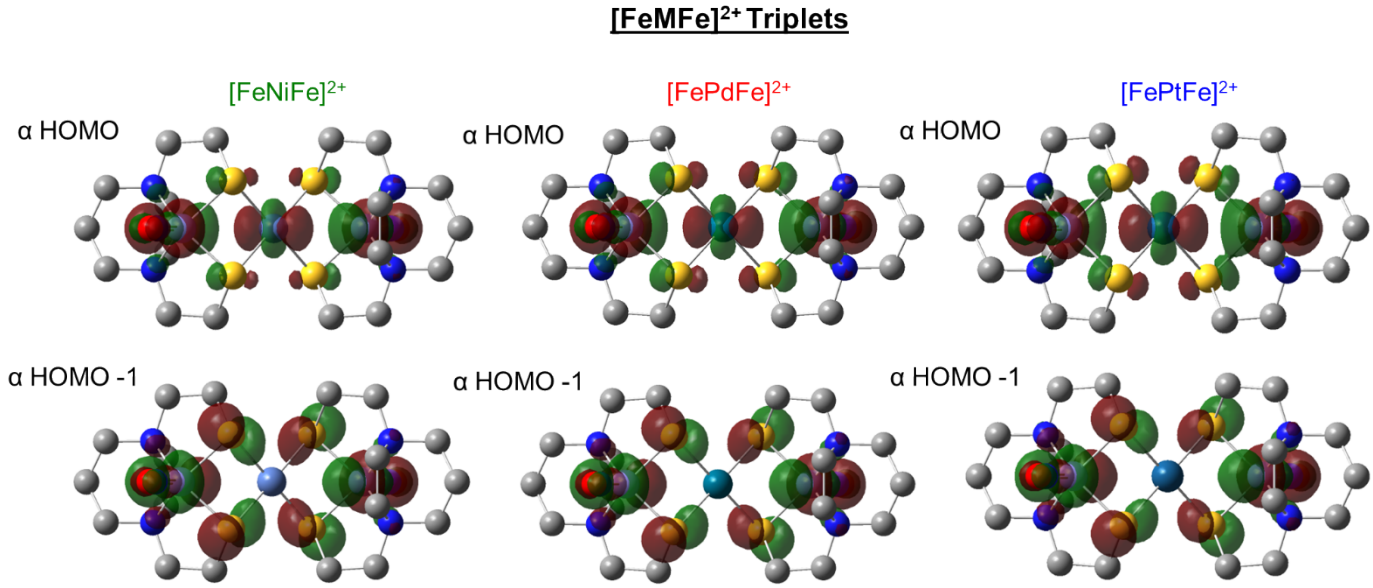

Figure S23. α HOMO and α HOMO-1 plots for the **[FeMFe]$^{2+}$** series in the triplet states (isovalue = 0.03).

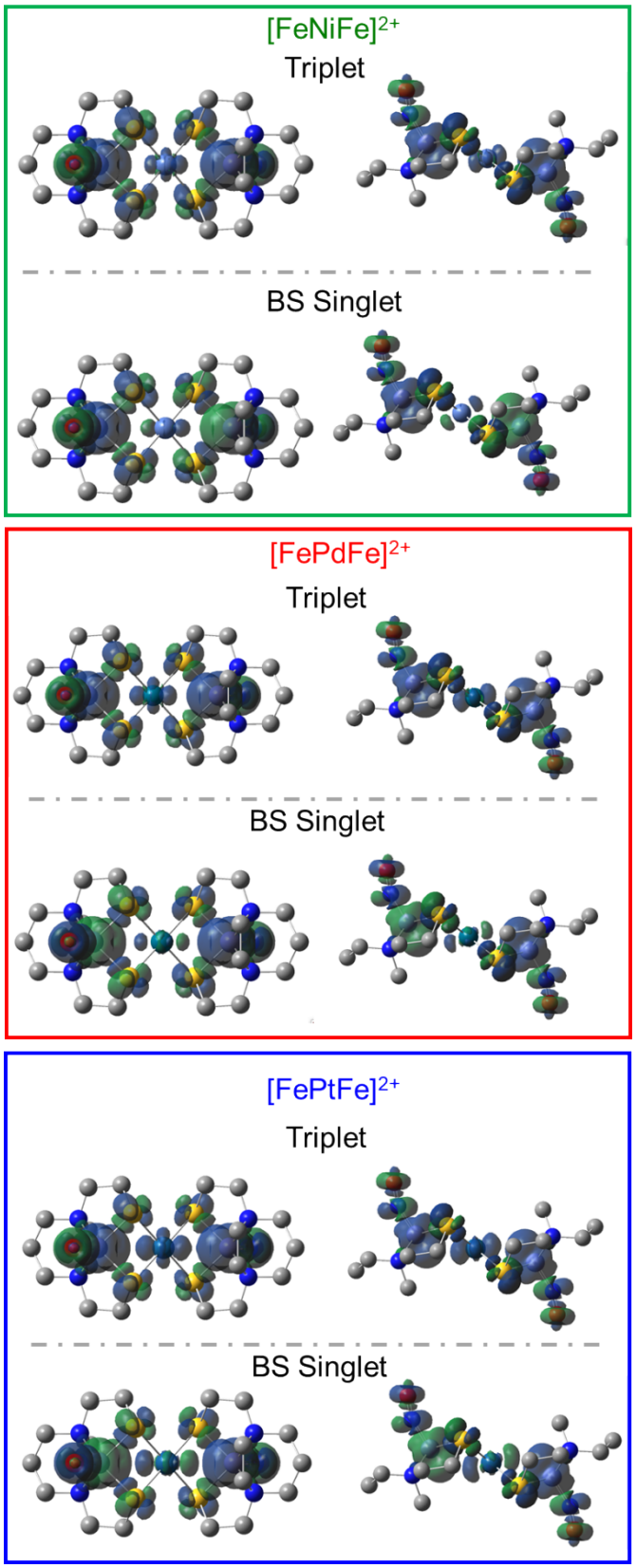

Figure S24. The two-view spin density plots of the **[FeMFe]$^{2+}$** series for the triplet and BS singlet states (isovalue = 0.001).

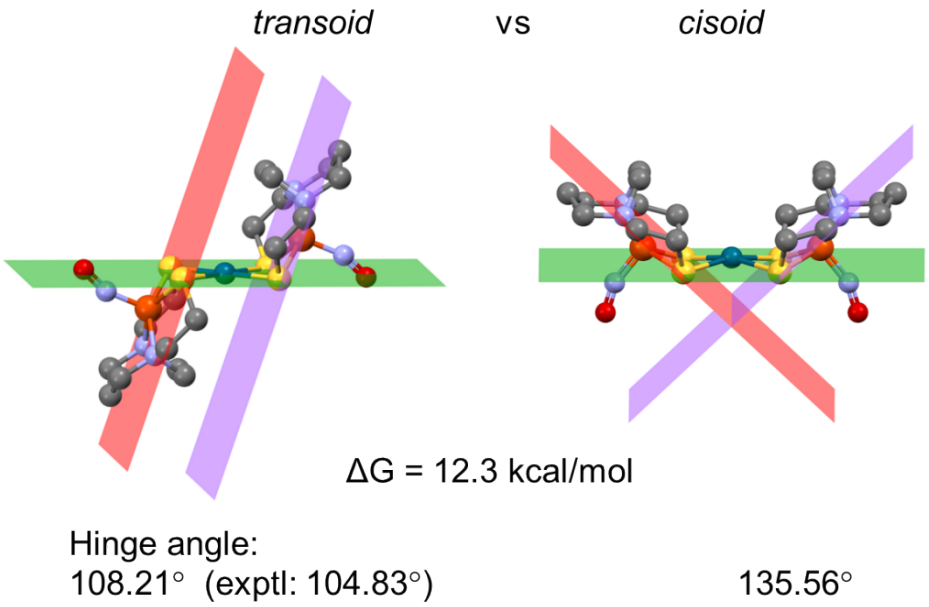

Figure S25. Comparison of the optimized transoid **[FePdFe]$^{2+}$** as isolated structure and the hypothetical optimized cisoid **[FePdFe]$^{2+}$** structure. The transoid structure is favored by 12.3 kcal/mol.

Computational Coordinates (optimized BS singlet)

[FeNiFe]$^{2+}$

Ni	0.00000894	0.00001219	-0.00000850
Fe	2.87501793	0.00009624	0.72361761
S	1.23803215	1.48809299	1.08283466
S	1.20576077	-1.44996261	1.14791876
N	3.64828627	1.26644845	-0.63607947
N	3.60084181	-1.31966860	-0.60483947
O	4.82428867	0.09975608	2.79189175
N	3.97752001	0.03167956	2.00117910
C	3.08226331	0.74532949	-1.92152067
H	3.63536715	1.06094756	-2.67959074
H	2.16370657	1.09300121	-2.04471899
C	3.05359415	-0.80830909	-1.90952324
H	2.12365204	-1.12582525	-2.02810839
H	3.59776930	-1.15786443	-2.65894846
C	3.15104460	-2.71677425	-0.31237200
H	3.67694673	-3.07024330	0.44823828
H	3.34033780	-3.28595289	-1.10012393
C	1.76513026	2.81921980	-0.08224373
H	1.25352088	2.74758307	-0.92684833
H	1.58175200	3.70636200	0.31695327
C	5.14973354	1.22925753	-0.67139690
H	5.49660451	1.35226493	0.24760700
H	5.47778380	1.98381209	-1.22193132
C	3.24035635	2.68121671	-0.36510584
H	3.47264464	3.24001705	-1.14864430
H	3.75131762	3.02140222	0.41156076
C	5.10259495	-1.33588175	-0.63628138
H	5.40605281	-2.11477092	-1.16667230
H	5.44359164	-1.44696312	0.28652234
C	1.68066563	-2.81644966	0.02121141
H	1.49507351	-3.68639646	0.45455855
H	1.14596118	-2.76429368	-0.81035768
C	5.69603068	-0.06579953	-1.23494401
H	6.67527524	-0.08103709	-1.09480051
H	5.53449932	-0.07549620	-2.21192342
Fe	-2.87500005	-0.00007186	-0.72363461
S	-1.23801426	-1.48806862	-1.08285166
S	-1.20574289	1.44998698	-1.14793577
N	-3.64831994	-1.26649436	0.63611149
N	-3.60087548	1.31962270	0.60487150
O	-4.82432235	-0.09980198	-2.79185973
N	-3.97750214	-0.03165518	-2.00119611
C	-3.08229698	-0.74537539	1.92155269
H	-3.63540082	-1.06099346	2.67962276
H	-2.16374025	-1.09304711	2.04475101
C	-3.05357628	0.80833346	1.90950624
H	-2.12368572	1.12577935	2.02814042
H	-3.59780297	1.15781852	2.65898048
C	-3.15107827	2.71672835	0.31240402
H	-3.67698041	3.07019740	-0.44820626
H	-3.34037147	3.28590699	1.10015595
C	-1.76511238	-2.81919543	0.08222673
H	-1.25350300	-2.74755871	0.92683133
H	-1.58178567	-3.70640790	-0.31692124
C	-5.14976721	-1.22930344	0.67142892
H	-5.49663817	-1.35231083	-0.24757498
H	-5.47781745	-1.98385800	1.22196334
C	-3.24039002	-2.68126261	0.36513786
H	-3.47267831	-3.24006295	1.14867633
H	-3.75135129	-3.02144812	-0.41152873
C	-5.10257708	1.33590612	0.63626438
H	-5.40603493	2.11479530	1.16665530
H	-5.44362530	1.44691722	-0.28649032
C	-1.68064775	2.81647403	-0.02122841
H	-1.49505563	3.68642083	-0.45457556
H	-1.14594330	2.76431804	0.81034068
C	-5.69601279	0.06582390	1.23492701
H	-6.67530889	0.08099119	1.09483254
H	-5.53453303	0.07545030	2.21195544

Computational Coordinates (optimized BS singlet)

[FePdFe]$^{2+}$

Pd	0.00000389	-0.00013310	0.00008123
Fe	-3.01569945	-0.00000760	0.68323720
S	-1.42061140	1.55110559	1.08719421
S	-1.42075105	-1.55127325	1.08715852
N	-3.89697068	1.30748583	-0.60661916
O	-4.04507091	0.00027223	3.29367784
N	-3.86543408	0.00012692	2.14031202
N	-3.89709007	-1.30740592	-0.60663875
C	-3.45923544	0.77832246	-1.94989738
H	-2.44202433	1.13662669	-2.12513925
H	-4.10516875	1.18678074	-2.73780969
C	-1.94074838	2.83383489	-0.16859934
H	-1.69477694	3.81715066	0.24290805
H	-1.36167892	2.68201550	-1.08241540
C	-3.44314455	2.72870088	-0.38421015
H	-3.97247956	3.07732693	0.50789852
H	-3.75975928	3.35012005	-1.23513867
C	-3.44339449	-2.72865958	-0.38424390
H	-3.76005956	-3.35003540	-1.23518442
H	-3.97274443	-3.07727269	0.50786631
C	-3.45931133	-0.77825406	-1.94990694
H	-4.10529452	-1.18663497	-2.73781746
H	-2.44213741	-1.13665412	-2.12517218
C	-5.40697448	1.28909960	-0.49250364
H	-5.80362770	2.14263610	-1.06035157
H	-5.63993360	1.43943702	0.56551269
C	-1.94100735	-2.83392143	-0.16866024
H	-1.36193193	-2.68212382	-1.08247748
H	-1.69512091	-3.81726999	0.24281832
C	-5.40709053	-1.28888219	-0.49250521
H	-5.64006066	-1.43919788	0.56551230
H	-5.80382953	-2.14238122	-1.06034981
C	-6.02670465	0.00013708	-1.03226113
H	-7.09079125	0.00018272	-0.76895288
H	-5.99384343	0.00013723	-2.12856121
Fe	3.01566808	-0.00004327	-0.68324616
S	1.42071519	-1.55136942	-1.08691183
S	1.42054070	1.55100843	-1.08727823
N	3.89714720	-1.30728101	0.60672672
O	4.04488472	-0.00055678	-3.29374795
N	3.86531652	-0.00027997	-2.14037139
N	3.89700186	1.30761042	0.60640923
C	3.45943670	-0.77798887	1.94996219
H	2.44227111	-1.13637159	2.12530775
H	4.10545543	-1.18628254	2.73788975
C	1.94105250	-2.83388398	0.16901776
H	1.69515608	-3.81727788	-0.24234779
H	1.36202017	-2.68200299	1.08284721
C	3.44345069	-2.72857065	0.38452832
H	3.97276907	-3.07725933	-0.50756574
H	3.76017725	-3.34984757	1.23551909
C	3.44314618	2.72878859	0.38385784
H	3.75979734	3.35030726	1.23469921
H	3.97240699	3.07734142	-0.50832886
C	3.45935874	0.77858763	1.94977256
H	4.10535057	1.18713369	2.73759029
H	2.44216060	1.13691004	2.12505552
C	5.40714281	-1.28875680	0.49251870
H	5.80391685	-2.14217909	1.06045388
H	5.64005399	-1.43920833	-0.56549193
C	1.94073513	2.83386739	0.16835019
H	1.36172893	2.68212304	1.08222026
H	1.69472098	3.81713861	-0.24323663
C	5.40699766	1.28922536	0.49218683
H	5.63988852	1.43942826	-0.56586410
H	5.80368480	2.14283768	1.05989735
C	6.02677598	0.00033848	1.03207066
H	7.09084644	0.00036661	0.76869716
H	5.99398229	0.00047667	2.12837263

Computational Coordinates (optimized BS singlet)

[FePtFe]$^{2+}$

Pt	-0.00001278	-0.00000144	0.00000078
Fe	-2.97527532	-0.00000157	0.69092128
S	-1.38184875	-1.55139714	1.12815207
S	-1.38184557	1.55139200	1.12815954
O	-4.06593135	-0.00000959	3.27663483
N	-3.83162177	-1.30694127	-0.61473921
N	-3.83162000	1.30694806	-0.61473148
N	-3.85512232	-0.00001566	2.12841299
C	-5.34391148	-1.28766095	-0.53568530
H	-5.60149284	-1.43556712	0.51703727
H	-5.72734014	-2.14248705	-1.11054153
C	-5.95053953	0.00000693	-1.09174287
H	-7.02083978	0.00000690	-0.85497243
H	-5.88991630	0.00001061	-2.18679779
C	-5.34390973	1.28766925	-0.53567491
H	-5.72733855	2.14250088	-1.11052221
H	-5.60148787	1.43556413	0.51704986
C	-3.36071182	-0.77849168	-1.94719394
H	-3.98602423	-1.18782053	-2.75118927
H	-2.33770102	-1.13319287	-2.09386875
C	-1.89164552	-2.84261234	-0.12762933
H	-1.29231732	-2.70069423	-1.02966415
H	-1.66295388	-3.82364228	0.29880682
C	-3.36071099	0.77850470	-1.94718979
H	-2.33769961	1.13320509	-2.09386130
H	-3.98602274	1.18783829	-2.75118294
C	-1.89163911	2.84261212	-0.12761955
H	-1.66294339	3.82363966	0.29882006
H	-1.29231299	2.70069512	-1.02965570
C	-3.38808689	-2.72838607	-0.37659377
H	-3.68829638	-3.35256777	-1.23148492
H	-3.93932481	-3.07129106	0.50446260
C	-3.38808161	2.72839219	-0.37658223
H	-3.93931767	3.07129599	0.50447560
H	-3.68829002	3.35257597	-1.23147203
Fe	2.97527264	0.00000258	-0.69091972
S	1.38184191	1.55139689	-1.12811854
S	1.38184008	-1.55139239	-1.12813216
O	4.06587374	0.00003674	-3.27665646
N	3.83164052	1.30693884	0.61473168
N	3.83164545	-1.30694912	0.61471509
N	3.85508816	0.00002642	-2.12843021
C	5.34392831	1.28766357	0.53564591
H	5.60148686	1.43557517	-0.51708146
H	5.72736670	2.14248814	1.11049795
C	5.95057155	-0.00000552	1.09168502
H	7.02086672	-0.00000136	0.85489149
H	5.88997213	-0.00001327	2.18674131
C	5.34393307	-1.28766807	0.53562615
H	5.72737596	-2.14250039	1.11046311
H	5.60148967	-1.43555975	-0.51710439
C	3.36076040	0.77848387	1.94719463
H	3.98608874	1.18781195	2.75117797
H	2.33775243	1.13318247	2.09389317
C	1.89164324	2.84259718	0.12767422
H	1.29233492	2.70066018	1.02971939
H	1.66293162	3.82363120	-0.29874182
C	3.36076462	-0.77851177	1.94718597
H	2.33775892	-1.13321716	2.09388231
H	3.98609689	-1.18784541	2.75116297
C	1.89164835	-2.84260491	0.12764638
H	1.66293604	-3.82363459	-0.29877917
H	1.29234255	-2.70067670	1.02969451
C	3.38809174	2.72838244	0.37660407
H	3.68831606	3.35256131	1.23149204
H	3.93930708	3.07129659	-0.50446284
C	3.38809787	-2.72839197	0.37657329
H	3.93931108	-3.07129541	-0.50449897
H	3.68832431	-3.35257861	1.23145455

References

1 C.-Y. Chiang, J. Lee, C. Dalrymple, M. C. Sarahan, J. H. Reibenspies and M. Y. Darensbourg, *Inorg. Chem.*, 2005, **44**, 9007–9016.

2 APEX4 "Program for Data Collection on Area Detectors" BRUKER AXS Inc., 5465 East Cheryl Parkway, Madison, WI 53711-5373 USA.

3 SADABS, Sheldrick, G.M. "Program for Absorption Correction of Area Detector Frames", BRUKER AXS Inc., 5465 East Cheryl Parkway, Madison, WI 53711-5373 USA.

4 O. V. Dolomanov, L. J. Bourhis, R. J. Gildea, J. a. K. Howard and H. Puschmann, *J. Appl. Cryst.*, 2009, **42**, 339–341.

5 G. M. Sheldrick, *Acta Cryst A*, 2015, **71**, 3–8.

6 G. M. Sheldrick, *Acta Cryst C*, 2015, **71**, 3–8.

7 A. L. Spek, *J Appl Cryst*, 2003, **36**, 7–13.

8 G. A. Bain and J. F. Berry, *J. Chem. Educ.*, 2008, **85**, 532.

9 N. F. Chilton, R. P. Anderson, L. D. Turner, A. Soncini and K. S. Murray, *J. Comput. Chem.*, 2013, **34**, 1164–1175.

10 D. T. Petasis and M. P. Hendrich, in *Methods in Enzymology*, eds. P. Z. Qin and K. Warncke, Academic Press, 2015, vol. 563, pp. 171–208.

11 Abragam, A.; Bleaney, B. Electron Paramagentic Resonance of Transition Ions. Oxford, **2012**; pp 1 - 944.

12 Gaussian 16, Revision C.01, Frisch, M. J.; Trucks, G. W.; Schlegel, H. B.; Scuseria, G. E.; Robb, M. A.; Cheeseman, J. R.; Scalmani, G.; Barone, V.; Petersson, G. A.; Nakatsuji, H.; Li, X.; Caricato, M.; Marenich, A. V.; Bloino, J.; Janesko, B. G.; Gomperts, R.; Mennucci, B.; Hratchian, H. P.; Ortiz, J. V.; Izmaylov, A. F.; Sonnenberg, J. L.; Williams-Young, D.; Ding, F.; Lipparini, F.; Egidi, F.; Goings, J.; Peng, B.; Petrone, A.; Henderson, T.; Ranasinghe, D.; Zakrzewski, V. G.; Gao, J.; Rega, N.; Zheng, G.; Liang, W.; Hada, M.; Ehara, M.; Toyota, K.; Fukuda, R.; Hasegawa, J.; Ishida, M.; Nakajima, T.; Honda, Y.; Kitao, O.; Nakai, H.; Vreven, T.; Throssell, K.; Montgomery, J. A., Jr.; Peralta, J. E.; Ogliaro, F.; Bearpark, M. J.; Heyd, J. J.; Brothers, E. N.; Kudin, K. N.; Staroverov, V. N.; Keith, T. A.; Kobayashi, R.; Normand, J.; Raghavachari, K.; Rendell, A. P.; Burant, J. C.; Iyengar, S. S.; Tomasi, J.; Cossi, M.; Millam, J. M.; Klene, M.; Adamo, C.; Cammi, R.; Ochterski, J. W.; Martin, R. L.; Morokuma, K.; Farkas, O.; Foresman, J. B.; Fox, D. J. Gaussian, Inc., Wallingford CT, **2016**.

13 J. Tao, J. P. Perdew, V. N. Staroverov and G. E. Scuseria, *Phys. Rev. Lett.*, 2003, **91**, 146401.

14 R. Krishnan, J. S. Binkley, R. Seeger and J. A. Pople, *The Journal of Chemical Physics*, 1980, **72**, 650–654.

15 A. D. McLean and G. S. Chandler, *The Journal of Chemical Physics*, 1980, **72**, 5639–5648.

16 T. Clark, J. Chandrasekhar, G. W. Spitznagel and P. V. R. Schleyer, *Journal of Computational Chemistry*, 1983, **4**, 294–301.

17 A. J. H. Wachters, *The Journal of Chemical Physics*, 1970, **52**, 1033–1036.

18 P. J. Hay, *J. Chem. Phys.*, 1977, **66**, 4377–4384.

19 K. Raghavachari and G. W. Trucks, *The Journal of Chemical Physics*, 1989, **91**, 1062–1065.

20 N. B. Balabanov and K. A. Peterson, *J. Chem. Phys.*, 2005, **123**, 064107.

21 K. A. Peterson, D. Figgen, M. Dolg and H. Stoll, *The Journal of Chemical Physics*, 2007, **126**, 124101.

22 D. Figgen, K. A. Peterson, M. Dolg and H. Stoll, *J. Chem. Phys.*, 2009, **130**, 164108.

23 GaussView, Version 6, Dennington, Roy; Keith, Todd A.; Millam, John M. Semichem Inc., Shawnee Mission, KS, **2016**.